Journal of The Electrochemical Society

OPEN ACCESS

Honeycomb Compound $Na_3Ni_2BiO_6$ as Positive Electrode Material in Na Cells

To cite this article: Lituo Zheng and M. N. Obrovac 2016 *J. Electrochem. Soc.* **163** A2362

Honeycomb Compound $Na_3Ni_2BiO_6$ as Positive Electrode Material in Na Cells

Lituo Zheng* **and M. N. Obrovac**,z**

Department of Chemistry, Dalhousie University, Halifax, Nova Scotia B3H 4R2, Canada

Honeycomb compound $Na_3Ni_2BiO_6$ was synthesized and studied as positive electrode material in sodium cells for the first time. This material exhibits a reversible capacity of ~80 mAh/g and an average voltage of ~3.1 V, corresponding to the reversible removal of half of the sodium from the structure. The sodiation/desodiation mechanism was studied by in situ X-ray diffraction and involves multiple phase transitions. It was observed that the phase transitions are different for the first charge/discharge processes, possibly due to kinetic hindrance. The multiple phase transitions may lead to sluggish kinetics that are responsible for the poor rate capability.
 [DOI: 10.1149/2.0991610jes]

Manuscript submitted June 27, 2016; revised manuscript received August 16, 2016. Published August 31, 2016.

Sodium ion batteries have attracted much attention in the past few years for their potential application in large scale grid storage.[1] Compared to lithium, sodium is more abundant and uniformly distributed on earth. The basic chemistry of sodium ion batteries is similar to that of lithium ion batteries, excepting that the active ion is sodium. The battery performance depends on the combined effects of the positive electrode, negative electrode, and electrolyte. Positive electrode material development is of importance to the commercialization of sodium ion batteries. Among many candidates for positive electrode materials, most research has been focused on layered sodium transition metal oxides.[2] These materials generally show good electrochemical performance and structural stability.[2] Nickel-based materials have been extensively studied as they offer high voltage and high capacity.[3–5] Partial substitution of Ni with other metals could modify the crystal structure and electrochemistry of these materials.[6] In the case of a binary $Na_xNi_yM_{1-y}{}^{z+}O_2$ (where x is usually between 2/3 and 1, M is a metal or metalloid) material, Ni usually exists as Ni^{2+} and its charge is balanced by M^{z+}, which has a higher oxidation state (z = 4, 5, or 6). Sodium intercalation/deintercalation operates on the Ni^{2+}/Ni^{4+} redox couple.[7] Using this strategy, the formation of the Ni^{3+} Jahn-Teller ion can be avoided in the synthesized pristine materials. Maximization of the active Ni^{2+} ion content of cathode materials is a strategy that may lead to higher energy density. In general, using notation proposed by Delmas et al.,[8] these layered-type materials can be grouped into two main categories: O3-type (Na+ in octahedral sites, ABCABC stacking) and P2-type (Na+ in prismatic sites, ABBA stacking). For a typical O3 material which has a sodium content of x = 1 or a typical P2 material which has a sodium content of x = 2/3, the relationships between y and z in $Na_xNi^{2+}{}_yM^{z+}{}_{1-y}O_2$ are given by

$$y\,(O3) = \frac{z-3}{z-2}$$

$$y\,(P2) = \frac{3z-10}{3z-6}$$

Apparently, having M with a high oxidation state will maximize the Ni^{2+} content. By using this strategy, researchers have studied O3-type $Na_3Ni^{2+}{}_2Sb^{5+}O_6$ ($NaNi_{2/3}Sb_{1/3}O_2$)[9,10] and P2-type $Na_2Ni^{2+}{}_2Te^{6+}O_6$ ($Na_{2/3}Ni_{2/3}Te_{1/3}O_2$)[11] as positive electrode materials for sodium ion batteries. In these materials, the Ni^{2+} contents were successfully enriched to 2/3, compared to 1/2 for O3-$NaNi_{1/2}Mn_{1/2}O_2$,[12] 1/3 for P2-$Na_{2/3}Ni_{1/3}Mn_{2/3}O_2$[7,13,14] and 1/4 for P2-$Na_{1/2}Ni_{1/4}Mn_{3/4}O_2$.[15] Notably, O3-type $Na_3Ni_2SbO_6$ shows high energy density and good rate capability.[9] $Na_3Ni_2SbO_6$ has a honeycomb structure that is generated by the 2:1 ordering of Ni^{2+} and Sb^{5+}. Recently, Yamada et al. reported that honeycomb-ordered Na_2RuO_3 could deliver extra capacity through the oxygen redox reaction, compared to the disordered Na_2RuO_3.[16] They observed an improvement of ~1/3 of the capacity in honeycomb-ordered Na_2RuO_3 than disordered Na_2RuO_3 (180 mAh/g and 135 mAh/g, respectively). These results show that the honeycomb structure is of interest for sodium ion battery positive electrode materials.

$Na_3Ni_2BiO_6$ was first synthesized and studied by Cava et al.[17] It has a honeycomb structure similar to that of $Na_3Ni_2SbO_6$. Cava et al. studied the structure and magnetic properties of this compound.[17] Here, we present a careful study of the electrochemistry of $Na_3Ni_2BiO_6$ honeycomb compound in Na cells, including the structural changes that occur during sodium removal and insertion.

Experimental

Stoichiometric amounts of NiO, $NaBiO_3$ and Na_2CO_3 powders were mixed by high energy ball milling using a SPEX 8000 mill. Typically a 3:1 ball:sample mass ratio with a sample size of ~5 g and three ~12.7 mm diameter stainless steel balls were milled for 2 hours. The obtained powders were then pelletized. The pellets were heated at 700°C for 8 hours first then 750°C for 12 hours in a tube furnace in oxygen to obtain $Na_3Ni_2BiO_6$. After cooling, samples were then immediately transferred to an Ar-filled glove box without air exposure.

Electrode preparation was carried out in an Ar-filled glove box because the material could be potentially air-sensitive. Electrodes consisted of active material, PVDF binder, carbon black in an 8:1:1 weight ratio. These components were mixed with an appropriate amount of N-methyl-2-pyrrolidone (Sigma Aldrich, anhydrous 99.5%) with two tungsten carbide balls in a Retsch PM200 rotary mill (100 rpm, 1 hour) to create a uniform slurry. Typically, ~0.4 g of active material was loaded in the milling jar for making slurry. The slurry was then coated onto aluminum foil with a coating bar having a 0.15 mm gap, and dried under vacuum at 80°C overnight. Circular electrodes were punched from the coating and incorporated into coin cells. 2325-type coin cells were assembled in an Ar-filled glove box. Na disks punched from thin foil (~0.4 mm) rolled from sodium ingot (Sigma Aldrich, ACS reagent grade) were used as counter/reference electrodes. Two Celgard 2300 and one blown microfiber separator (3M Company) were used as separators. 1 M $NaPF_6$ (Aldrich, 98%) in a solution of ethylene carbonate (EC), diethyl carbonate (DEC) and monofluoroethylene carbonate (FEC) (volume ratio 3:6:1, from BASF) was used as electrolyte. Cells were cycled with a Maccor Series 4000 Automated Test System (Maccor Inc., Tulsa OK). The ambient cycling temperature was 30.0°C (±0.1°C).

*Electrochemical Society Student Member.
**Electrochemical Society Member.
zE-mail: mnobrovac@dal.ca

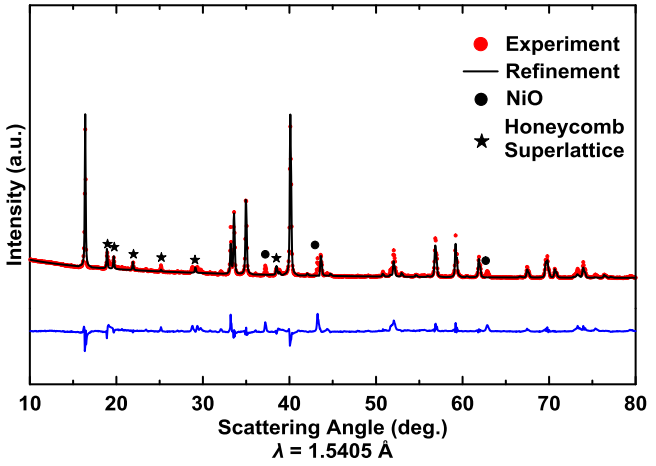

Figure 1. X-ray diffraction pattern for synthesized $Na_3Ni_2BiO_6$ and its Rietveld refinement.

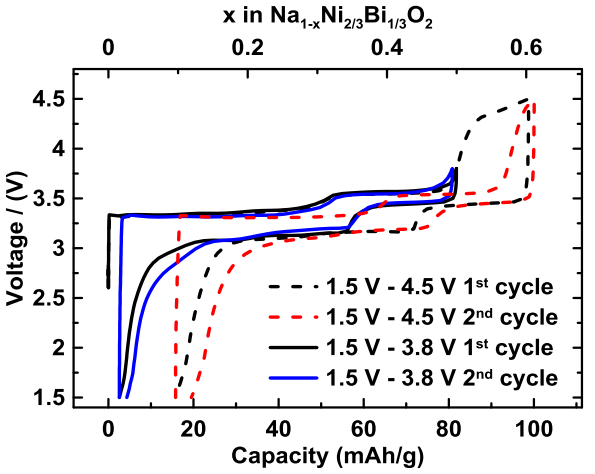

Figure 3. Voltage curves of $Na_3Ni_2BiO_6$ at C/20 current density for the first 2 cycles in the voltage range of 1.5 V – 3.8 V and 1.5 V – 4.5 V.

X-ray diffraction (XRD) patterns were measured with a Rigaku Ultima IV X-ray diffractometer equipped with a Cu anode X-ray tube and dual detectors. A D/TeX Ultra linear detector with a K-beta filter was used to measure XRD patterns of powder samples and in situ coin cells. Powder samples were loaded into a gastight X-ray sample holder (DPM Solutions, Hebbville NS) in an argon-filled glove box to avoid air contamination. A coin cell modified to have a thin beryllium window inset in the cell can was used for in situ XRD measurements. For such cells, electrode slurry made using the same procedure as described above was coated directly onto the beryllium window using a 0.3 mm coating bar. After drying overnight at 80°C under vacuum, the beryllium window was then affixed in the cell bottom can using Roscobond adhesive. In situ coin cells were then constructed using the same procedure as described above. In situ cells were cycled at a rate of C/10 for 2 cycles, first cycle between 1.5 V–3.8 V and second cycle between 1.5 V–4.5 V. Phase observed in in situ XRD data were compared to previously reported in situ XRD results of similar O3-type materials, such as $NaNi_{0.5}Mn_{0.5}O_2$,[12] Na_2RuO_3,[16] and $Na_3Ni_2SbO_6$.[9] A scintillation detector with a diffracted beam monochromator was used to measure ex situ XRD patterns. For ex situ XRD studies, coin cells were prepared as described above, but were stopped at different cutoff voltages after trickle at constant voltage to achieve equilibrium. Electrodes for ex situ XRD measurements were recovered from these cells in an argon glove box, and the electrode materials were scraped off the aluminum foil and washed with dimethyl carbonate (DMC, BASF) several times. The recovered electrode materials were then transferred to a zero-background silicon wafer and sealed in the gastight sample holder for the ex situ XRD measurements. Rietveld refinements were conducted using Rietica software.

Results and Discussion

Figure 1 shows the XRD pattern of synthesized $Na_3Ni_2BiO_6$. The XRD pattern was found to be similar to that reported previously.[17] The structure resembles the α-$NaFeO_2$ structure, except for low angle peaks caused by the honeycomb superlattice ordering in the transition metal layer. The monoclinic space group C2/m has been used by researchers to describe this type of honeycomb structure.[17] Here, the honeycomb structure is generated by the 2:1 ordering of edge sharing NiO_6 and BiO_6 in the *a*-*b* plane, as shown in Figure 2. In the *a*-*b* plane, every BiO_6 octahedron is surrounded by six NiO_6 octahedra, thus forming a honeycomb ordering. A small amount of an NiO impurity phase was also present in the XRD pattern (indicated by solid circles). Atttempts to completely remove this phase by changing synthesis conditions were not successful. Rietveld refinement gives the lattice parameters $a = 5.399$ Å, $b = 9.345$ Å, $c = 5.674$ Å and $\beta = 108.402°$, which are in close approximation to the values reported by Cava et al.[17]

Figure 3 shows the voltage curve of $Na_3Ni_2BiO_6$ for the first 2 cycles in the voltage range of 1.5 V – 3.8 V and 1.5 V – 4.5 V, respectively. Figure 4 shows the corresponding differential capacity curves of the same cells. $Na_3Ni_2BiO_6$ was found to have a first charge capacity of ∼82 mAh/g when cycled between 1.5 V and 3.8 V. This capacity of ∼82 mAh/g corresponds to the removal of ∼1.5 Na per $Na_3Ni_2BiO_6$. It should be noted that the heavy atomic weight of Bi

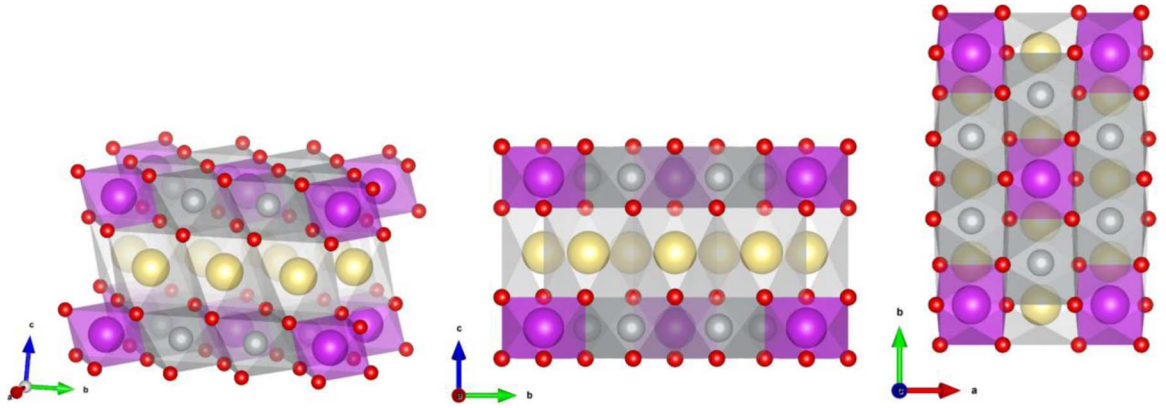

Figure 2. Structure of Structure of $Na_3Ni_2BiO_6$. Sodium is shown in yellow, oxygen in red, bismuth in gray, and nickel in purple.

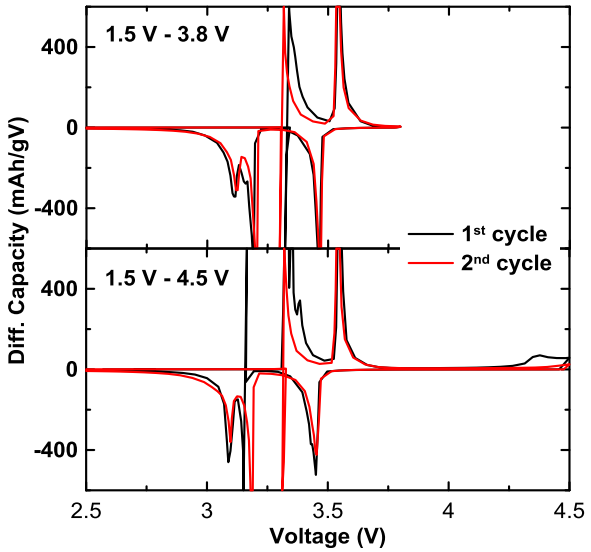

Figure 4. Differential capacity curve of $Na_3Ni_2BiO_6$ cells at a scan rate of C/20 between 1.5 V – 3.8 V and 1.5 V – 4.5 V (vs. Na^+/Na).

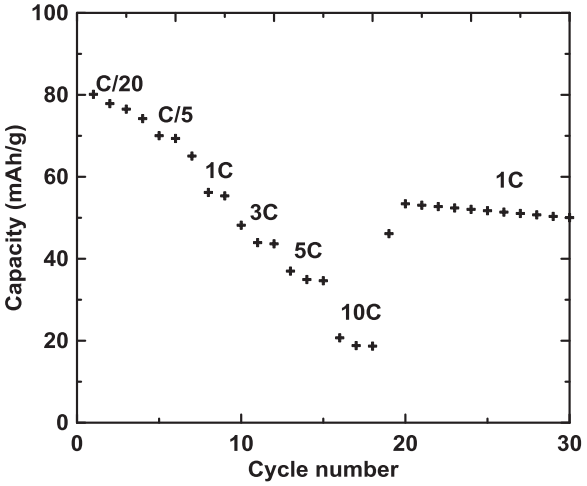

Figure 5. Rate capability of the material at constant charge/discharge rates of C/20–10 C.

inevitably lowers the gravimetric capacity, however its volumetric energy density is comparable to other Na-ion cathode materials. The volumetric capacity of $Na_3Ni_2BiO_6$ is calculated to be 1557 Wh/L, based on a bulk density of 6.0012 g/ml from XRD measurements. For comparison, the volumetric capacity of $NaCrO_2$ is estimated to be ~1570 Wh/L (120 mAh/g at ~3 V).

The voltage curve is characterized by two flat plateaus during charge. The two plateaus in the voltage curve correspond to two sharp peaks in the differential capacity centered at ~3.3 V and ~3.55 V. This redox potential is typical for layered sodium nickelates.[4] For example, P2-$Na_{2/3}Ni_{1/3}Mn_{2/3}O_2$[7,13,14] also has two plateaus at ~3.3 V and ~3.6 V. These plateaus are due to Na^+/vacancy ordering and/or phase transitions, as suggested by previous reports.[13,14] In this study, assuming the starting material has a composition corresponding to x = 3 in $Na_xNi_2BiO_6$, the charge capacity associated with these two plateaus corresponds to the theoretical formation of $Na_{1.5}Ni_2BiO_6$ at 3.8 V. If the cell is subsequently discharged, both the two plateaus are completely reversible with a hysteresis of ~0.2 V. The first discharge capacity is ~79 mAh/g with a very small irreversible capacity (~3 mAh/g). The first cycle coulombic efficiency is ~96%. The lower plateau during discharge is actually composed of two small plateaus, as can be seen from the two successive peaks at ~3.1 V and ~3.2 V in the differential capacity curve. When the cell was cycled between 1.5 V – 4.5 V, another plateau with a capacity of ~17 mAh/g appears at ~4.4 V upon charge. However this plateau is not reversible, as can be seen by the similar discharge curve to that of cell cycled between 1.5 V – 3.8 V. Below 3.8 V the differential capacity curve is nearly identical for the cells cycled in the two voltage ranges. The first discharge capacity is ~83 mAh/g, only slightly higher than that of cell cycled between 1.5 V – 3.8 V. This leads to an irreversible capacity of ~16 mAh/g and a low first cycle coulombic efficiency (~84%). After the first cycle, this high voltage plateau disappears and the charge capacity decreases to 84 mAh/g. The average discharge voltage is ~3.16 V vs. Na^+/Na.

$Na_3Ni_2SbO_6$ has been shown to exhibit a superior rate capability by Yang et al.[9] At 10C rate, the capacity reached 104 mAh/g, which exceeds 85% of its capacity at C/10 (117 mAh/g). Unfortunately, the rate capability for $Na_3Ni_2BiO_6$ is less attractive. Figure 5 shows the rate performance of $Na_3Ni_2BiO_6$. As can be seen in the figure, the reversible capacity drops significantly with increasing current rate. At 1C rate, a capacity of ~55 mAh/g was observed, corresponding to ~70% of the C/20 capacity. When the rate was increased to 5C, less than 50% of capacity is retained. The poor rate performance indicates slow kinetics and low sodium ion conductivity. When the current density increases, the capacity is limited by the kinetic barrier of sodium diffusion in the active material. Yang et al. attributed the superior rate capability of $Na_3Ni_2SbO_6$ to the weaker attraction force between sodium and the structure.[9] The average bond length of Na-O in $Na_3Ni_2SbO_6$ is 2.434 Å, larger than that in $Na_3Ni_2BiO_6$ (2.395 Å).[11] This might also explain the inferior rate capability of $Na_3Ni_2BiO_6$. A longer bond length may indicate a weaker bonding strength, and therefore a more facile intercalation/deintercalation of sodium ions.

In order to understand the structural changes during sodium extraction/insertion, in situ XRD experiments were performed. Figure 6 shows the XRD patterns of a $Na_3Ni_2BiO_6$ in situ XRD cell during the first 2 cycles, where the first cycle is between 1.5 – 3.8 V and the second cycle is between 1.5 – 4.5 V, respectively. The XRD patterns at the end of each charge or discharge are shown with red lines. Some of the peaks in the XRD patterns are caused by cell parts, such as beryllium and beryllium oxide from the beryllium window. These peaks could be easily identified as their positions and intensities do not shift during

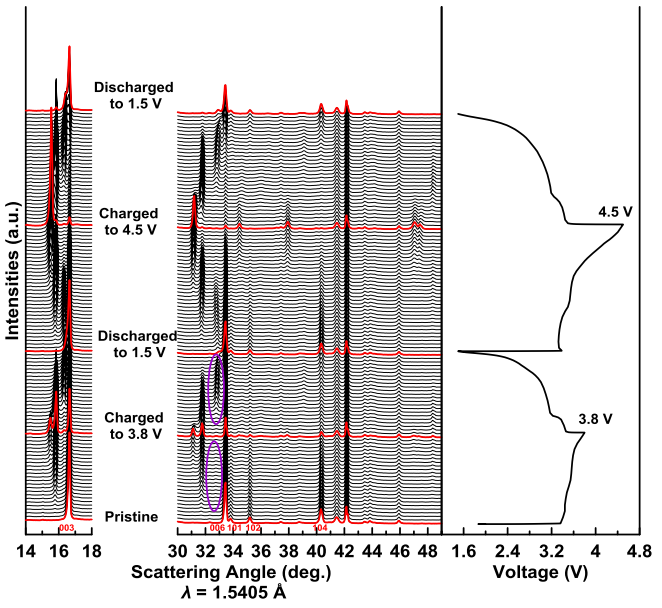

Figure 6. In situ XRD patterns of the $Na_3Ni_2BiO_6$ electrode at various charge/discharge state during the first two cycles (1.5 V – 3.8 V and 1.5 V – 4.5 V). Phase transitions are different for the first charge/discharge processes, as can be seen by the regions shown in purple ovals.

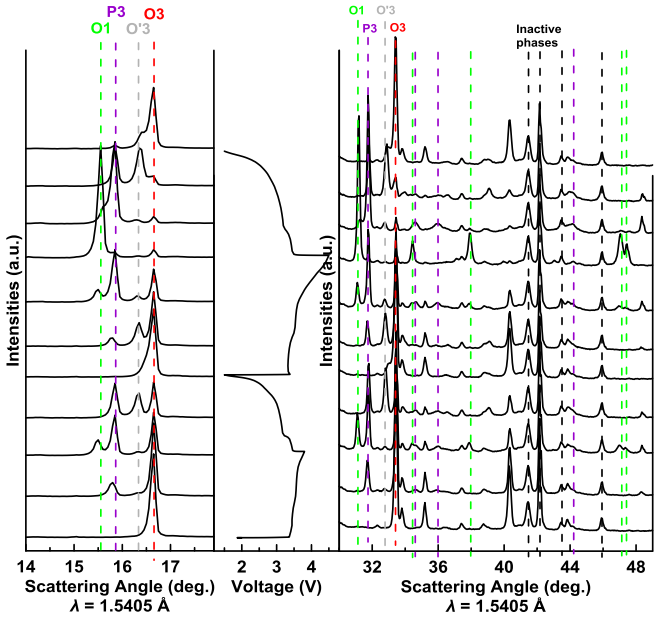

Figure 7. Enlarged in situ XRD patterns of the $Na_3Ni_2BiO_6$ electrode at various charge/discharge state during the first two cycles (1.5 V – 3.8 V and 1.5 V – 4.5 V).

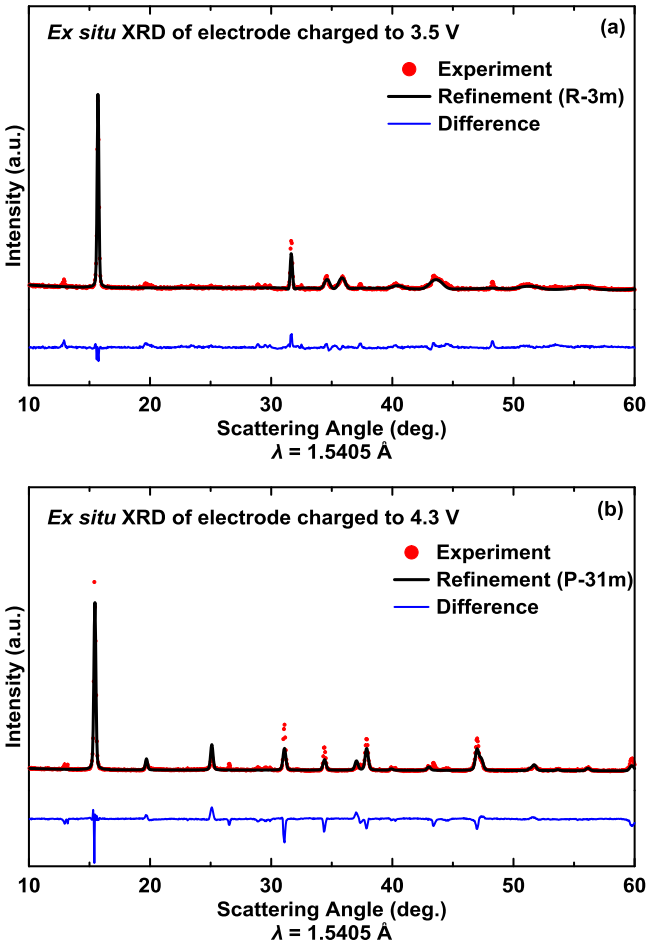

Figure 8. Ex situ XRD patterns and Rietveld refinements of electrodes charged to (a) 3.5 V and (b) 4.5 V.

the charge and discharge process. The initial XRD pattern is that of $Na_3Ni_2BiO_6$. Miller indexes are indicated for each peak. During cycling the XRD peaks barely shift during the charge/discharge process. Instead peaks disappear and peaks from new phases appear during each plateau indicating multiphase processes. This will be discussed in detail below.

Overall, there are four major peak positions in the 2θ range of 14° – 18°, corresponding to four different phases (O3, O'3, P3, O1). Enlarged in situ XRD patterns at selected states of charge/discharge are shown in Figure 7. It was found that the phase transitions that occur during charge and discharge are different during the first cycle. In the 2θ range of 32° – 33° (shown in two purple ovals for the first charge/discharge in Figure 6, respectively), only very small peaks could be observed during the first charge, yet large peaks appear and disappear during the first discharge process in this region. The low peak intensity during first charge could be due to kinetic hindrance in phase formation. In the first charge process, the O3 phase transforms into the P3 phase directly. According to Yang and co-workers' report on $Na_3Ni_2SbO_6$,[9] the P3 phase corresponds to the formation of $Na_2Ni_2SbO_6$ with space group of C2/m. Accordingly, in the case of $Na_3Ni_2BiO_6$, we speculate that the P3 phase should be $Na_2Ni_2BiO_6$. The desodiation capacity also supports the formation of $Na_2Ni_2BiO_6$. When the intensity of the P3 phase is at its highest, the desodiation capacity corresponds to the removal of ∼1.35 Na per $Na_3Ni_2SbO_6$ (corresponding to a final stoichiometry of about $Na_{1.95}Ni_2BiO_6$). At the end of charging to 3.8 V, some diffraction peaks of the O1 phase also appears. This O3-P3-O1 transition agrees well with past observations of $Na_3Ni_2SbO_6$ during charge.[7] It should be noted that even at the end of charging to 3.8 V, there is still significant amount of the pristine O3 phase remaining in the structure. Such phenomenon is indicative of the slow kinetics. During the first discharge process, the O1 phase starts to disappear, but instead of transforming to the O3 phase from the P3 phase, the P3 phase first transforms into a monoclinic O'3 phase, then the O'3 phase gradually disappears and a hexagonal O3 phase is formed. As discussed above, the formation of the O'3 phase during the first charge is hindered due to kinetic limitations. When the material was discharged to 1.5 V, it transforms back to O3 phase and the XRD pattern looks almost identical to that of the pristine material.

After the first cycle, the material was then charged to 4.5 V. Unlike the first cycle, the material undergoes an O3-O'3-P3-O1 process during the second cycle, indicating that the structure is stabilized after the first cycle. When the $Na_3Ni_2BiO_6$ was charged to 4.5 V, all the diffraction lines can be indexed to an O1 phase. Yang et al. reported that the O1 phase corresponds to a further removal of one Na from the P3-type $Na_2Ni_2SbO_6$ lattice and the formation of of $NaNi_2SbO_6$ with $P\bar{3}$ 1m symmetry.[7] In the case of $Na_3Ni_2BiO_6$, the O1 phase should correspond to the formation of $NaNi_2BiO_6$, which agrees well with the desodiation capacity: at the end of second charge, the capacity is ∼90 mAh/g, corresponding to the removal of ∼1.7 Na per $Na_3Ni_2BiO_6$. The following discharge follows the course of O1-P3-O'3-O3. At the end of discharge the material almost fully converts to O3 with a small amount of O'3 phase left, as can be seen by the small shoulder at ∼16.4°.

Another pronounced feature with this material is that there are several three-phase regions during cycling. Two-phase regions are dictated by thermodynamics for the number of degrees of freedom available to this system and are commonly observed for the sodium ion battery positive electrode materials during sodium extraction/insertion.[4] The coexistence of three phases during cycling has not been reported to the best of our knowledge. This three-phase phenomenon indicates sluggish kinetics and poor sodium ion diffusion, as discussed above. The sluggish kinetics hinders the material's ability to undergo phase transitions. This can also explain the poor rate performance for this material. To confirm the hypothesis of the slow kinetics, ex situ XRD was performed. Coin cells were charged/discharged to indicated voltages and held at the voltage for 30 hours to achieve equilibrium. Figure 8a shows the ex situ XRD pattern and Rietveld refinement of an electrode charged to 3.5 V. The XRD pattern was well-fitted with a P3 structure. Figure 8b shows the ex situ XRD pattern and Rietveld

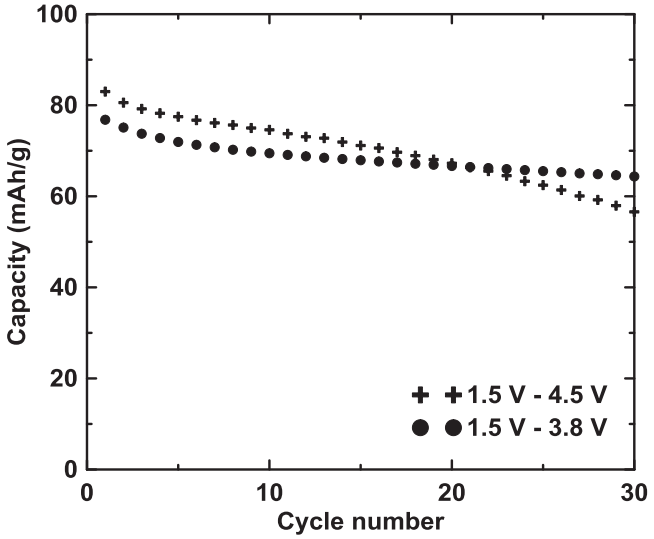

Figure 9. Cycling performance of $Na_3Ni_2BiO_6$ electrodes cycled at different voltage ranges at C/20 rate.

refinement of an electrode charged to 4.5 V and the XRD was fitted with an O1 structure. Therefore, it can be concluded that the plateau before 3.5 V corresponds to the phase transition to P3 phase, and the plateau above 3.5 V corresponds to the phase transition to the O1 phase.

Compared to the multiple phases observed in in situ XRD, only single phases was present in the ex situ XRD patterns. This confirms the hypothesis the slow kinetics hindering phase transitions, and the phase transition process of O3-P3-O1. However, we were unable to obtain the single O'3 phase by ex situ XRD, as there is not distinct boundary between O3 and O'3 phases. This might be because the sodium diffusion gradients cause the plateaus to merge. Nevertheless, what is clear is that the formation potential of the O'3 phase is between O3 and P3 phases, as can be seen from the in situ XRD data. It is also observed that the peak positions of O'3 phase change slightly during charge/discharge process. The position shift of O'3 peaks indicates a single-phase region in the equilibrium phase diagram. However, the peak shift is accompanied by the appearance/disappearance of O'3, O3, P3 and O1 phases, implying multiphase coexistence. Such a contradiction exists because the system is in a non-equilibrium state due to kinetic hindrance. Phase transitions and Na^+/vacancy ordering have been associated with capacity fade and poor reversibility during cycling.[18] One strategy to address this issue is to introduce disorder in transition metal layers by partial substitution. Wang et al.[19] and Singh[20] studied the Mg substitutued Na-Ni-Mn-O system and they found that the addition of Mg effectively suppress the P2-O2 phase transition and improve the capacity retention for P2-$Na_{2/3}Ni_{1/3}Mn_{2/3}O_2$. Kim et al.[21] and Meng et al.[22] used Li substitution in the Na-Ni-Mn-O system and achieved good cyclability.

Figure 9 shows the cycling performance of $Na_3Ni_2BiO_6$. When cycled between 1.5 – 4.5 V, the capacity retention is ~75% after 25 cycles. By restricting the voltage range of 1.5 – 3.8 V at C/20 rate, $Na_3Ni_2BiO_6$ retained 85% of its intial discharge capacity after 25 cycles. Previously, $Li_3Ni_2BiO_6$ has been synthesized using similar high temperature solid state reaction process by Subramanian et al.[23] Subramanian et al. also studied the electrochemical performance of $Li_3Ni_2BiO_6$ in a lithium half-cell. They reported a first discharge capacity of 81.7 mAh/g,[23] which is comparable to the capacity we obtained for $Na_3Ni_2BiO_6$. However, a rapid capacity fade was observed for $Li_3Ni_2BiO_6$ and after 10 cycles a capacity of only 22 mAh/g was retained. Similarly, Meng et al. reported the synthesis and electrochemical properties of $Li_3Ni_2SbO_6$ in 2007.[24] The first charge/discharge capacities of $Li_3Ni_2SbO_6$ are 110/92 mAh/g, which are comparable to that of $Na_3Ni_2SbO_6$ (122/117 mAh/g) reported by Yang et al.[9] Nevertheless, after 10 cycles, the reversible capacity of $Li_3Ni_2SbO_6$ drops rapidly to ~38 mAh/g, while $Na_3Ni_2SbO_6$ shows a good cycling performance (95% capacity retention after 50 cycles). Meng et al. studied the Ni migration during $Li_3Ni_2SbO_6$ cycling by XRD and calculations.[24] They attributed the drastic capacity fade to the structure degradation caused by the interlayer cation mixing of Li/Ni during cycling. The migration of Ni into the Li layer not only reduces the available sites for Li but also blocks lithium diffusion pathways. It is well-known that Li/Ni mixing is common in the cathode materials for lithium ion batteries due to the similar ionic size of Li and Ni,[25] while the mixing of Ni and Na is usually negligible due to the large difference of ion sizes of Na^+(1.02 Å) and Ni^{2+}(0.69 Å). We believe this is can explain the better cycling performance of $Na_3Ni_2SbO_6$ and $Na_3Ni_2BiO_6$ compared to their lithium counterparts.

Conclusions

$Na_3Ni_2BiO_6$ was synthesized using a conventional high temperature solid-state reaction and its electrochemistry was studied for the first time. When cycled between 1.5 V – 3.8 V, this material has two voltage plateaus at ~3.1 V and ~3.4 V and a first discharge capacity of ~80 mAh/g with negligible irreversible capacity, corresponding to the reversible removal of ~1.5 Na per $Na_3Ni_2SbO_6$. It was found by in situ XRD that the first charge proceeds via an O3-P3-O1 phase transition, while the phase transitions during the first discharge proceed as O1-P3-O'3-O3. After the first cycle, the material was stabilized and a reversible O3-O'3-P3-O1 phase transitions occur during cycling. The sluggish phase transitions and poor rate capability indicate slow kinetics of this material. It was also observed that cycling is significantly better for $Na_3Ni_2SbO_6$ and $Na_3Ni_2BiO_6$ in Na cells compared to their Li counterparts in Li cells. This is attributed to the lack of cation mixing during cycling of the Na-containing oxides.

Acknowledgments

The authors acknowledge funding from NSERC and 3M Canada, Co. under the auspices of the Industrial Research Chair and Discovery grant programs.

References

1. N. Yabuuchi, K. Kubota, M. Dahbi, and S. Komaba, *Chem. Rev.*, **114**, 11636 (2014).
2. M. H. Han, E. Gonzalo, G. Singh, and T. Rojo, *Energy Environ. Sci.*, **8**, 81 (2015).
3. P. Vassilaras, X. Ma, X. Li, and G. Ceder, *J. Electrochem. Soc.*, **160**, A207 (2012).
4. J. Molenda and A. Stoklosa, *Solid State Ionics*, **38**, 1 (1990).
5. J. J. Braconnier, C. Delmas, and P. Hagenmuller, *Mater. Res. Bull.*, **17**, 993 (1982).
6. R. Fielden and M. N. Obrovac, *J. Electrochem. Soc.*, **161**, A1158 (2014).
7. H. Yoshida, N. Yabuuchi, K. Kubota, I. Ikeuchi, A. Garsuch, M. Schulz-Dobrick, and S. Komaba, *Chem. Commun.*, **50**, 3677 (2014).
8. C. Delmas, C. Fouassier, and P. Hagenmuller, *Physica B+C*, **99**, 81 (1980).
9. D. Yuan, X. Liang, L. Wu, Y. Cao, X. Ai, J. Feng, and H. Yang, *Adv. Mater.*, **26**, 6301 (2014).
10. J. Ma, S.-H. Bo, L. Wu, Y. Zhu, C. P. Grey, and P. G. Bruce, *Chem. Mater.*, **27**, 2387 (2015).
11. A. Gupta, C. Buddie Mullins, and J. B. Goodenough, *J. Power Sources*, **243**, 817 (2013).
12. S. Komaba, N. Yabuuchi, T. Nakayama, A. Ogata, T. Ishikawa, and I. Nakail., *Inorg. Chem.*, **51**, 6211 (2012).
13. Z. Lu and J. R. Dahn, *J. Electrochem. Soc.*, **148**, A1225 (2001).
14. D. H. Lee, J. Xu, and Y. S. Meng, *Phys. Chem. Chem. Phys.*, **15**, 3304 (2013).
15. P. Manikandan, D. Ramasubramonian, and M. M. Shaijumon, *Electrochim. Acta*, **206**, 199 (2016).
16. B. Mortemard de Boisse, G. Liu, J. Ma, S. Nishimura1, S.-C. Chung, H. K, Y. Harada, J. Kikkawa, Y. Kobayashi, M. Okubo, and A. Yamada, *Nat. Commun.*, **7**, 11397 (2016).
17. E. M. Seibel, J. H. Roudebush, H. Wu, Q. Huang, M. N. Ali, H. Ji, and R. J. Cava, *Inorg. Chem.*, **52**, 13605 (2013).
18. R. J. Clément, P. G. Bruce, and C. P. Grey, *J. Electrochem. Soc.*, **162**, A2589 (2015).
19. P.-F. Wang, Y. You, Y.-X. Yin, Y.-S. Wang, L.-J. Wan, L. Gu, and Y.-G. Guo, *Angew. Chemie Int. Ed.*, **55**, 7445 (2016).
20. G. Singh, N. Tapia-Ruiz, J. M. Lopez del Amo, U. Maitra, J. W. Somerville, A. R. Armstrong, J. Martinez de llarduya, T. Rojo, and P. G. Bruce, *Chem. Mater.*, **28**, 5087 (2016).

21. D. Kim, S.-H. Kang, M. Slater, S. Rood, J. T. Vaughey, N. Karan, M. Balasubramanian, and C. S. Johnson*Adv. Energy Mater.*, **1**, 333 (2011).
22. J. Xu, D. H. Lee, R. J. CleÉment, X. Yu, M. Leskes, A. J. Pell, G. Pintacuda, X.-Q. Yang, C. P. Grey, and Y. S. Meng, *Chem. Mater.*, **26**, 1260 (2014).
23. R. Berthelot, W. Schmidt, S. Muir, J. Eilertsen, L. Etienne, A. W. Sleight, and M. A. Subramanian, *Inorg. Chem.*, **6**, 5377 (2012).
24. X. Ma, K. Kang, G. Ceder, and Y. S. Meng, *J. Power Sources*, **173**, 550 (2007).
25. Z. Lu, D. D. MacNeil, and J. R. Dahn, *Electrochem. Solid-State Lett.*, **4**, A200 (2001).